Journal of Structural Geology, Vol. 14, No. 5, pp. 565 to 577, 1992
Printed in Great Britain

0191-8141/92 $05.00 + 0.00

Evolution of a salt-related listric growth fault near the D-1 well, block 5605, Danish North Sea: displacement history and salt kinematics

K. PETERSEN,* O. R. CLAUSEN and J. A. KORSTGÅRD

Geologisk Institut, Aarhus Universitet, C. F. Møllers Allé, 8000 Aarhus C, Denmark

(*Received* 3 *July* 1991; *accepted in revised form* 24 *November* 1991)

Abstract—The Top Chalk surface and the Tertiary sediments of the Danish North Sea are cut by only a few major faults which are often related to or controlled by the mobile Zechstein salt. A single listric growth fault (the D-1 fault) and its adjacent area have been mapped in detail in order to unravel the fault geometry and kinematics. The spatial distribution of displacements and lateral dimensions of the fault are used to examine the interaction between salt movements and the evolution of the fault.

The displacement distribution on the fault is systematic, with contours of equal displacement forming concentric semi-ellipses centred on the point of maximum displacement with displacement decreasing upwards and laterally approaching the displacement configuration for the upper part of an ideal simple blind fault. Furthermore, within the volume surrounding the fault vertical displacement shows similar contour patterns for the hangingwall and footwall, respectively.

The lateral displacement variation during fault growth and reconstructed displacement geometries indicate that footwall uplift was mainly a result of salt flow. Despite the complicated nature of salt dynamics the evolution of the D-1 fault resulted in a systematic fault displacement geometry within the rock volume surrounding the fault.

INTRODUCTION

THE displacement geometry analysis of a simple blind planar fault (Watterson 1986, Barnett *et al.* 1987, Walsh & Watterson 1987, 1988, 1989, 1991, Gibson *et al.* 1989) shows that the displacement on a fault is systematic and forms an elliptical contour pattern. Reverse drag in both hangingwall and footwall is generated at planar faults because of the distribution of strain in the volume containing the fault (Barnett *et al.* 1987) (Fig. 1).

Listric normal faults are steep near the surface and flatten at depth. Hamblin (1965) showed that a listric normal fault creates a roll-over structure (reverse drag) in the hangingwall block. Several models for the geometrical relations between hangingwall deformation, fault plane geometry and hangingwall displacement velocity field have been proposed in recent years (e.g. Crans *et al.* 1980, White *et al.* 1986, Williams & Vann 1987, Waltham 1989, White & Yielding 1991), but none take any motion or deformation of the footwall into account.

Listric normal faults in sedimentary basins are often associated with layers of low viscosity materials such as overpressured shales or salt forming the detachment horizon. Flow of the low viscosity materials or escape of excess fluids may influence or control the fault development (e.g. Bruce 1973, Daily 1976, Ewing 1983, Jenyon 1986, 1988).

Growth faults are normal faults across which there is an abrupt thickening of stratigraphic units from the footwall side to the hangingwall side and with a corresponding downwards increase in horizon displacement. Thus, a necessary condition for the evolution of a growth fault is progressive sedimentation contemporaneous with fault movement, resulting in thickening of hangingwall beds towards the fault plane.

At any given moment, the amount of finite, horizontal extension along the fault increases downwards, from a minimum at the free surface, to a maximum along the new horizontal detachment surface. While bedding at the free surface is horizontal, the tilt of the bed segments increases downwards due to extension and fault growth. Because of the geometry of listric faults the angle between bedding and the fault plane decreases with depth as the fault plane flattens with depth. The final shape of a growth fault results from a combination of (i) initial curvature, (ii) differential compaction and (iii) deformation of the fault plane due to diapirism of salt or shale.

Here we investigate a salt-related listric growth fault in order to unravel the displacement history of the fault and the relation between fault development and kinematics of the underlying salt. Using available geophysical data (mainly seismic), detailed two-way time maps of selected horizons have been produced in order to develop a model for the displacement geometry of the investigated fault. In particular we have studied the influence of salt movement on the fault displacement geometry with special emphasis on reverse drag in the footwall block. Evaluation of hydrocarbon prospectivity of fault-related potential plays requires a detailed knowledge of the displacement history and geometry of the fault.

The fault we have chosen for a detailed study, called the D-1 fault, is located in the northern part of the Danish North Sea sector on the north slope of the Ringkøbing–Fyn High (Fig. 2). The fault has a width of

*Current address: Department of Geological Sciences, University of South Carolina, Columbia, SC 29208, U.S.A.

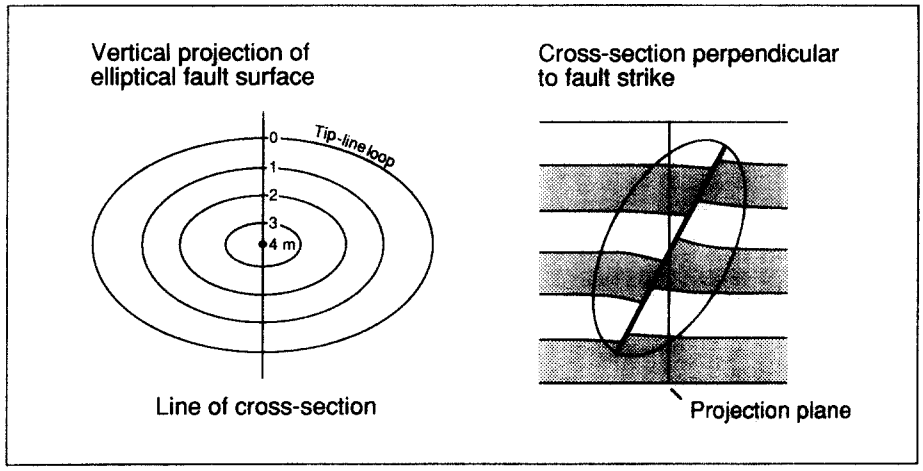

Fig. 1. Displacement distribution in cross-section and fault plane projection of a simple ideal blind fault (after Barnett *et al.* 1987).

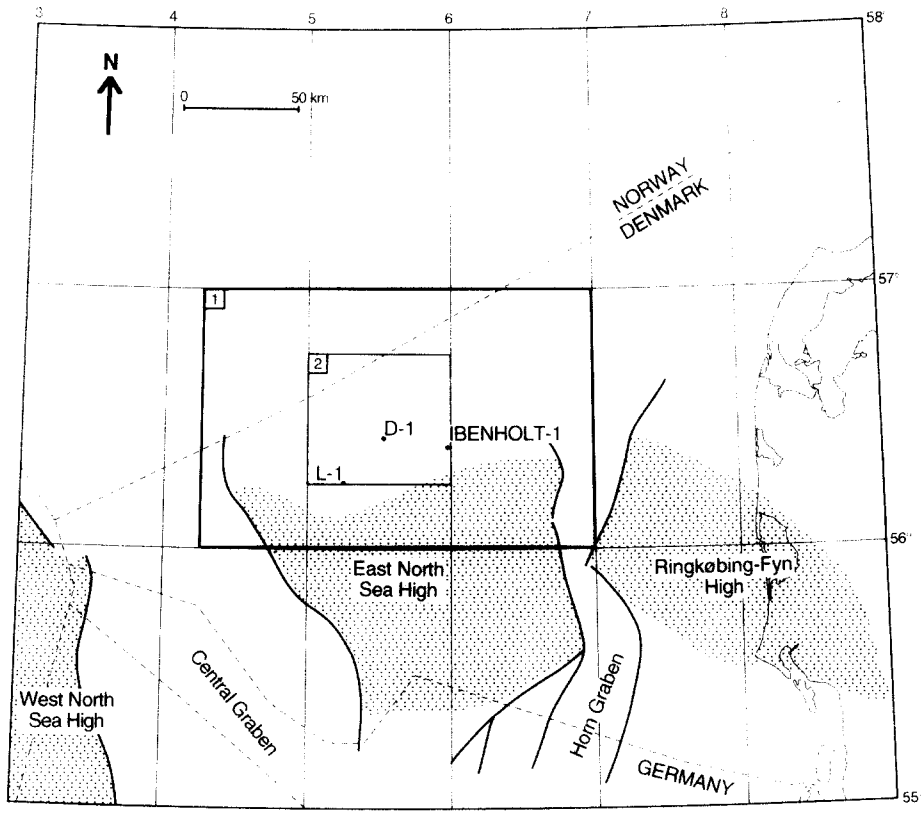

Fig. 2. The outline of the Danish North Sea sector showing the location of subsequent maps: (1) Figs. 3, 5, 7 and 8; (2) Figs. 6, 13, 14 and 15 (after Frandsen *et al.* 1987; Vejbæk 1990). The fault investigated in this study is penetrated by the D-1 well.

about 70 km and has an ENE–WSW orientation with downthrow to the north-northwest (Fig. 3). It offsets Triassic to Tertiary sediments and detaches along the upper surface of the Zechstein salt. Three seismic lines normal to the D-1 fault are shown in Fig. 4 with the general stratigraphy indicated. The Zechstein salt has been periodically mobile since Mid-Triassic times and rests on a basement of Rotliegendes volcanics. Jurassic and Lower Cretaceous sequences are very thin in the area. Three wells are located near the fault (Fig. 2) and one of these, the D-1 well, penetrates the fault (Figs. 2 and 4).

The D-1 fault appears in several publications (Michelsen & Andersen 1981, Ziegler 1982, Gowers & Sæbøe 1985) and on the Tectonic Map of the North Sea (GECO 1989) as a major NNW-dipping fault cutting the Top Chalk surface and the Lower Tertiary sediments (C1–C3). On previously published maps the fault appears with widely differing lengths and curvature in map view.

DEPTH MAPS

The mapping is based on interpretations on the two-dimensional seismic surveys RTD-81, SP-82, CGT-81 and DCS-81 which together form a grid of sufficient

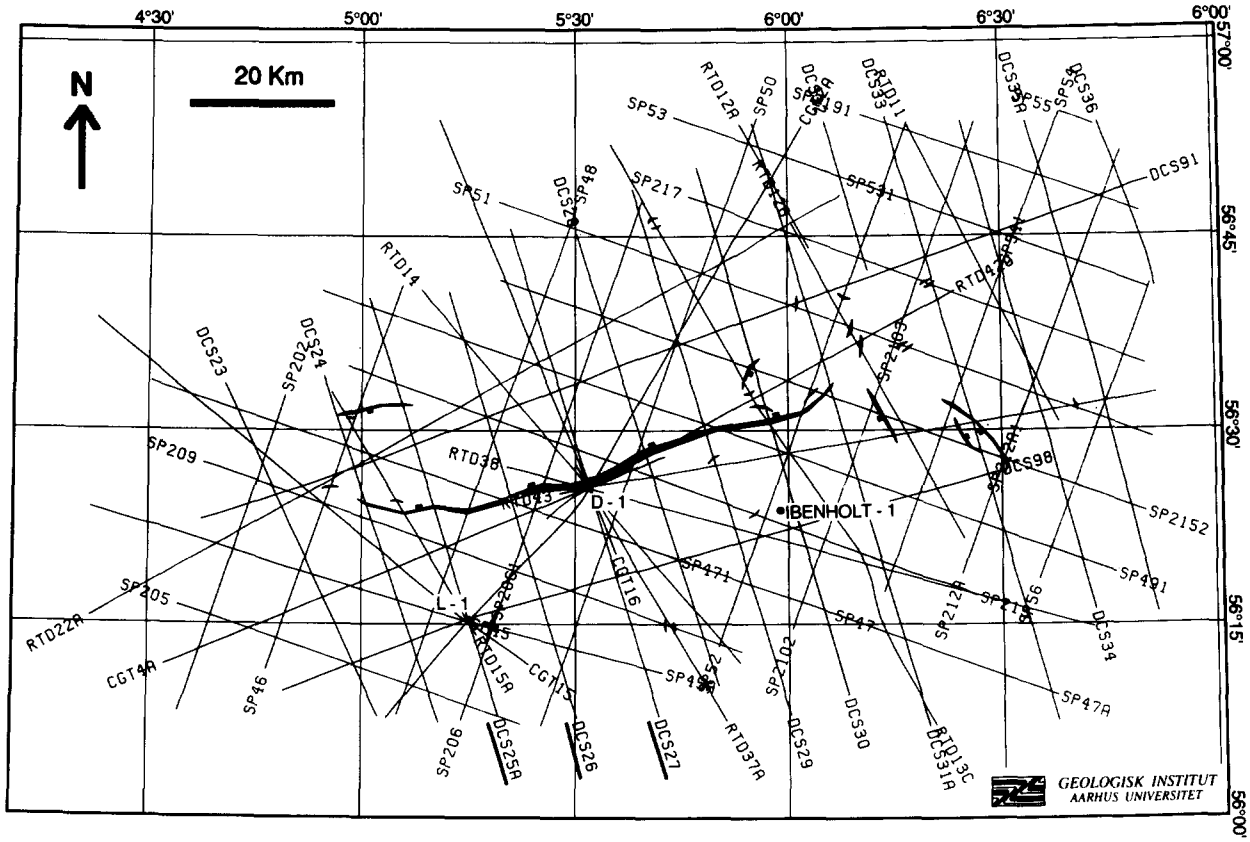

Fig. 3. The seismic grid in the mapped area. The seismic data consist of the surveys SP-82, RTD-81, CGT-81 and DCS-81. The D-1 fault is shown at the Top Chalk level. The location of the seismic lines DCS-25A, DCS-26 and DCS-27 appearing in Fig. 4 are indicated, underlined.

density to tie the mapped horizons across and around faults (Fig. 3). The mapped horizons are dated as shown in Fig. 4 through a correlation with biostratigraphic subdivisions of the D-1 and the L-1 wells (Cater *et al.* 1968, Church *et al.* 1970) and the lithostratigraphic subdivision from the Well Data Summary Sheets published by the Geological Survey of Denmark.

The Top pre-Zechstein surface (Fig. 5) is cut by a number of faults none of which cuts the stratigraphically younger horizons. One of the faults however, is roughly similar in position, extent and map view to the D-1 fault, but is separated from the D-1 fault by the Zechstein salt. The Top pre-Zechstein surface has a regional ENE–WSW trend with a dip to the NNW.

The Top Zechstein is only mapped in the areas close to the D-1 fault (Fig. 6) and corresponds to the top of the mobile salt. The topography of the Top Zechstein surface is the result of salt movement that generated an elongate salt ridge parallel to the trend of the major fault on the Top pre-Zechstein surface. The salt ridge is asymmetric with a steep slope towards the north and a shallower slope to the south. The regional trend of the Top Zechstein surface is parallel to that of the Top pre-Zechstein surface.

The only major fault cutting the Top Chalk surface (Fig. 7) is the ENE–WSW-striking D-1 fault. The fault plane dips to the NNW. The contours of the Top Chalk surface have a NNW trend with a slope to the WSW and with a marked topographic high located above the major salt accumulation (Fig. 6).

The pattern of the D-1 fault on the C2 (Intra Early Miocene) surface (Fig. 8) is similar to the fault pattern at the Top Chalk horizon. However, close to the D-1 fault a few antithetic normal faults have appeared and the western part of the fault has been disconnected from the main fault. The C2 surface dips uniformly to the SW.

CONSTRUCTION OF CONTOUR DISPLACEMENT DIAGRAMS

The problem of fault correlation in seismic interpretation is well known. A procedure to perform this objectively is by construction of contour displacement diagrams. Contour diagrams of equal displacement have been shown to be an efficient way of analysing fault displacements and they impose valuable constraints on seismic interpretation (cf. Barnett *et al.* 1987, Freeman *et al.* 1990, Chapman & Meneilly 1991). The reliability of horizon correlation across and along faults and fault systems is important in the study of basin tectonics and crucial to the analysis of fault-related reservoir formation in petroleum exploration.

Contour displacement diagrams are constructed according to the method described by Barnett *et al.* (1987) and Freeman *et al.* (1990). In this study, the vertical displacement of a mapped horizon is measured on the seismic sections for all mapped horizons displaced by the D-1 fault and posted on a vertical projection plane parallel to the mean fault strike (strike-projection) (Fig.

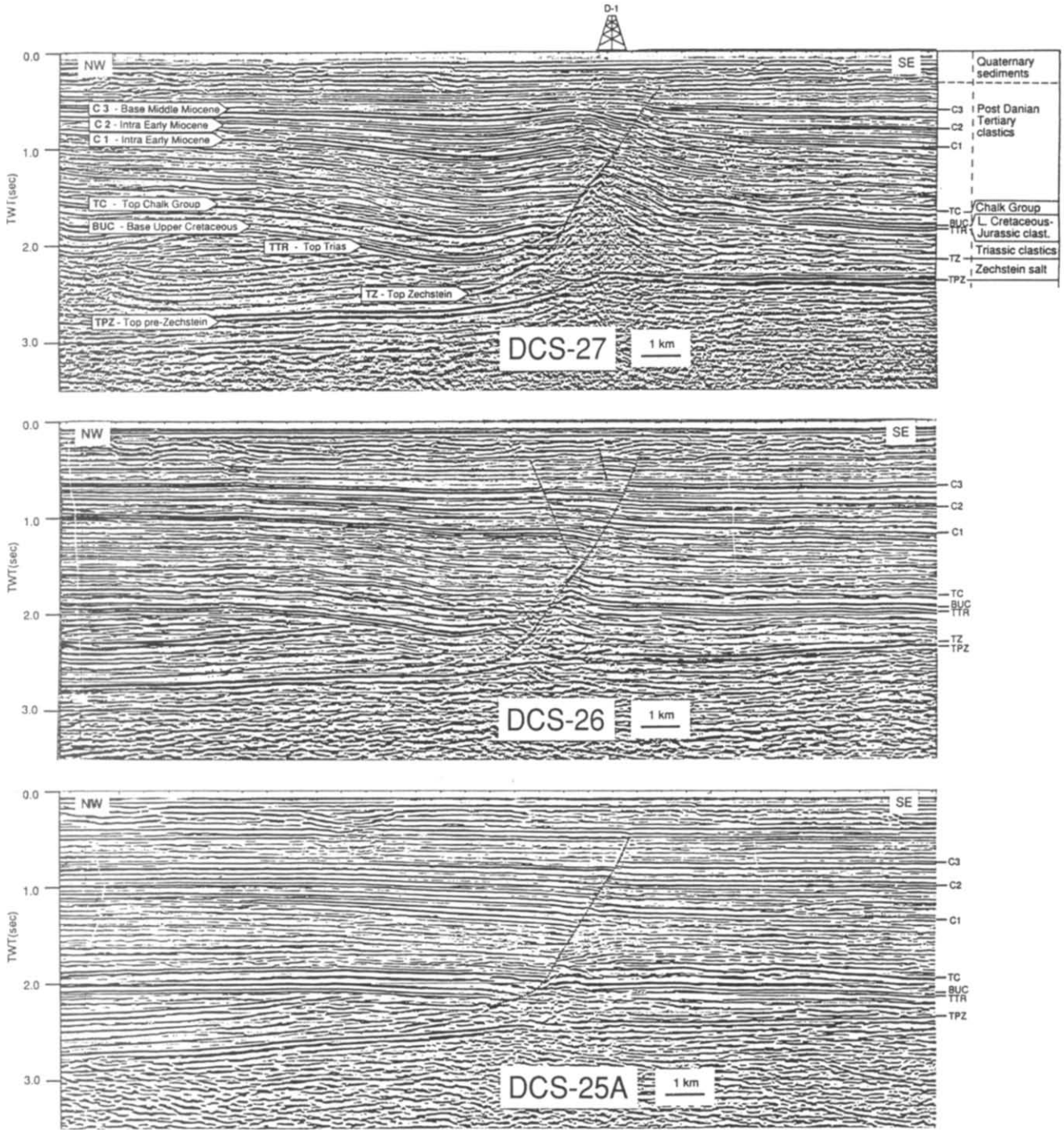

Fig. 4. Part of the seismic lines DCS-25A, DCS-26 and DCS-27 across the D-1 fault. The line DCS-27 passes through the D-1 well. The mapped reflectors and their ages are shown. Note the uplift of the footwall and the hangingwall roll-over structure on line DCS-27. Moving southwestwards, the uplift and the roll-over become less significant. For location of the seismic lines, see Fig. 3.

9). The displacement values are posted at the intersection between the strike-projection and the interpreted 'regional' (i.e. regional dip) of the different horizons (Fig. 9). The regional is interpreted using the structure contour maps of the different horizons as discussed later. The vertical displacement values posted on the strike-projection are contoured to show the variation in throw along the fault.

To investigate the change in displacement pattern during the evolution of a normal fault, the contour displacement pattern can be constructed for any time in the past by using a 'fault displacement backstripping-technique'. To construct the contour displacement diagrams the vertical displacement of a horizon is subtracted from the displacement of the underlying horizons. The sedimentary layers are then removed permitting the horizons below to be corrected for the regional regional subsidence since deposition of the chosen horizon (Fig. 10).

The observed offset of the youngest mapped horizon consists of three major components: (1) the incremental displacement in the hangingwall of the youngest pre-

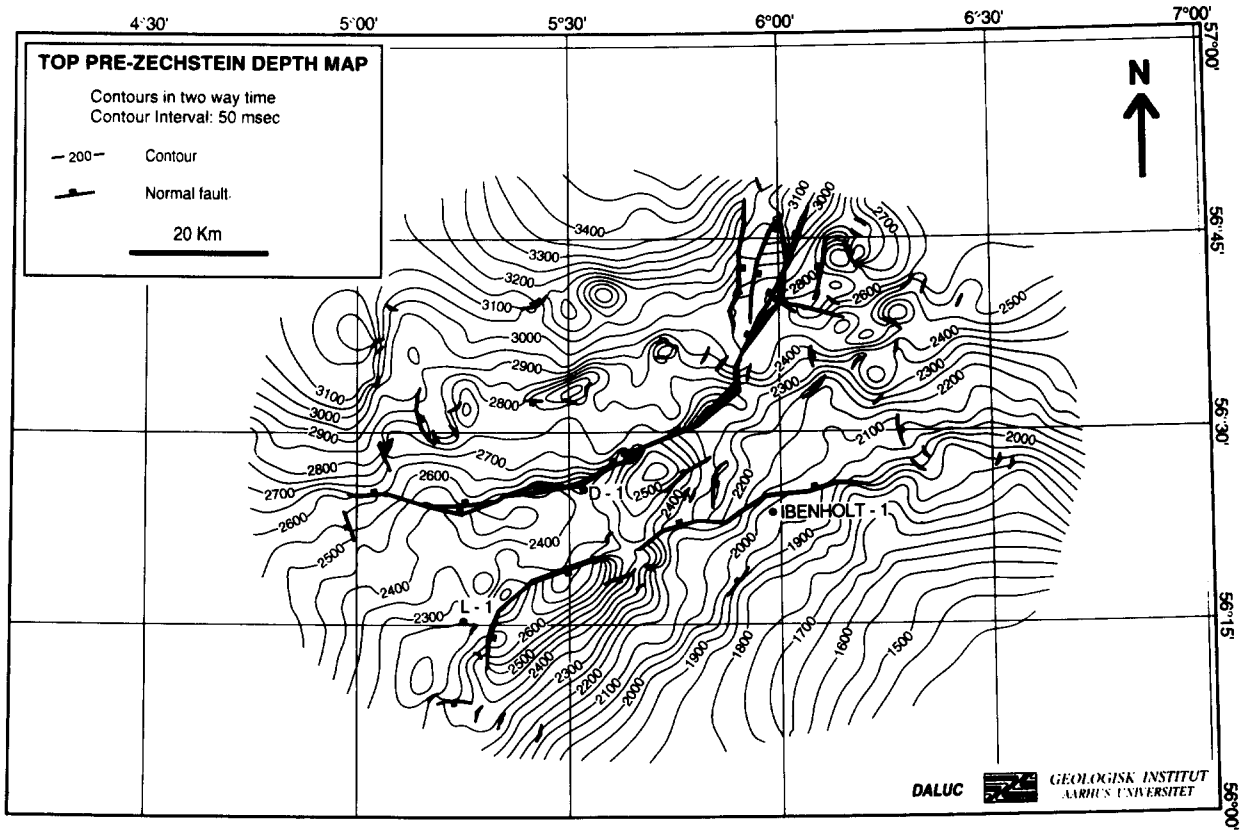

Fig. 5. Two-way time depth map to the Top pre-Zechstein.

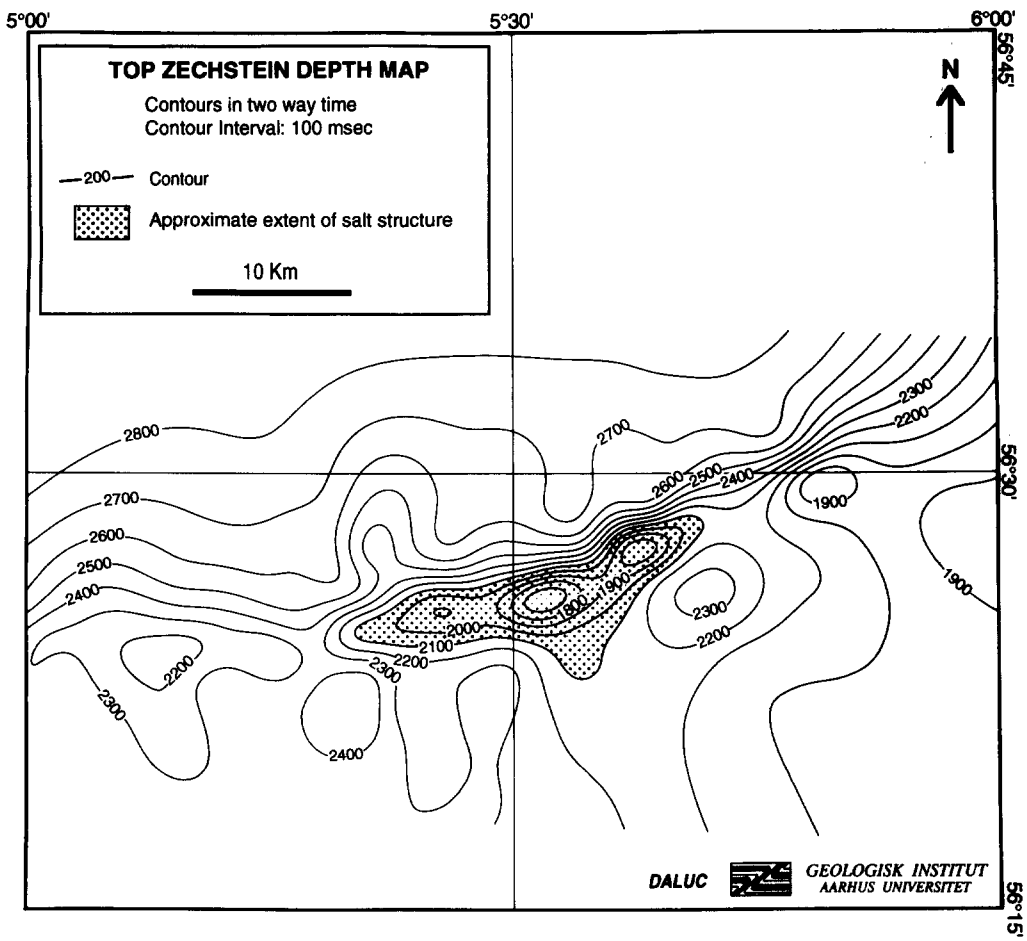

Fig. 6. Two-way time depth map to Top Zechstein. Note that this map only shows part of the previous maps.

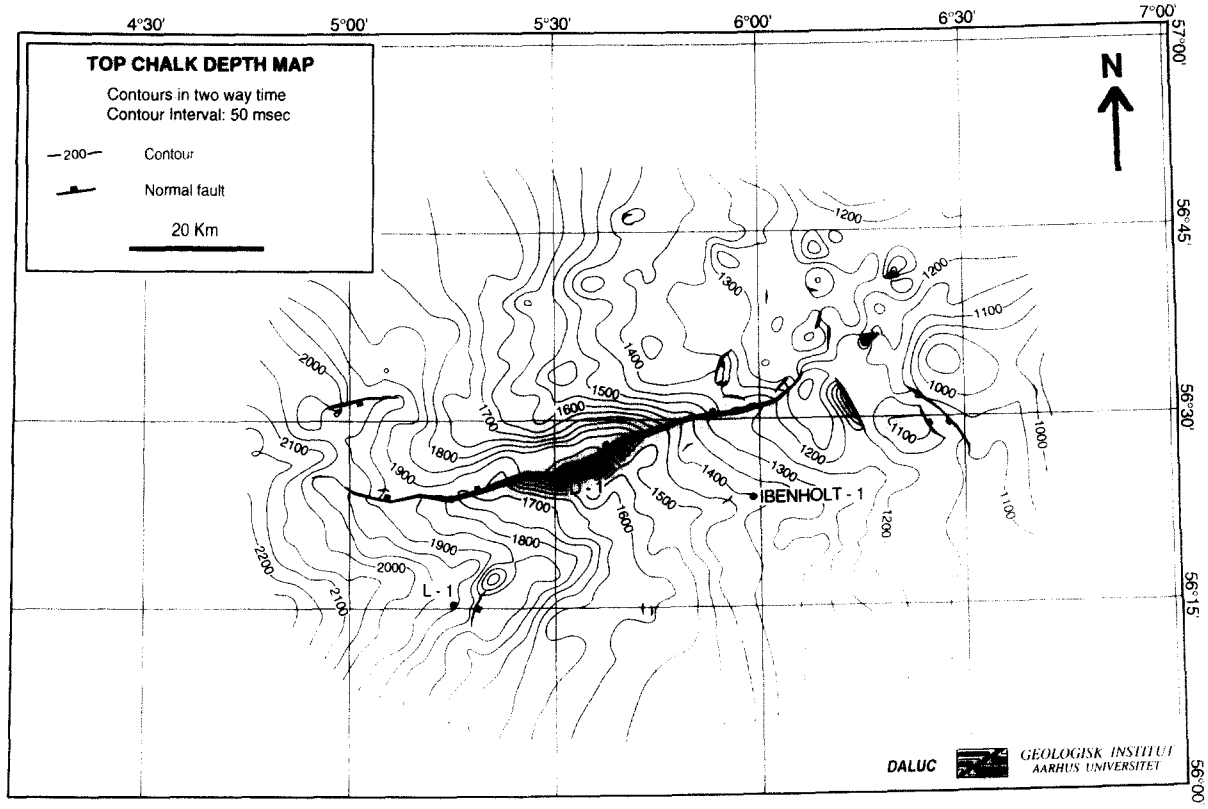

Fig. 7. Two-way time depth map to the Top Chalk surface. The major fault shown is the D-1 fault.

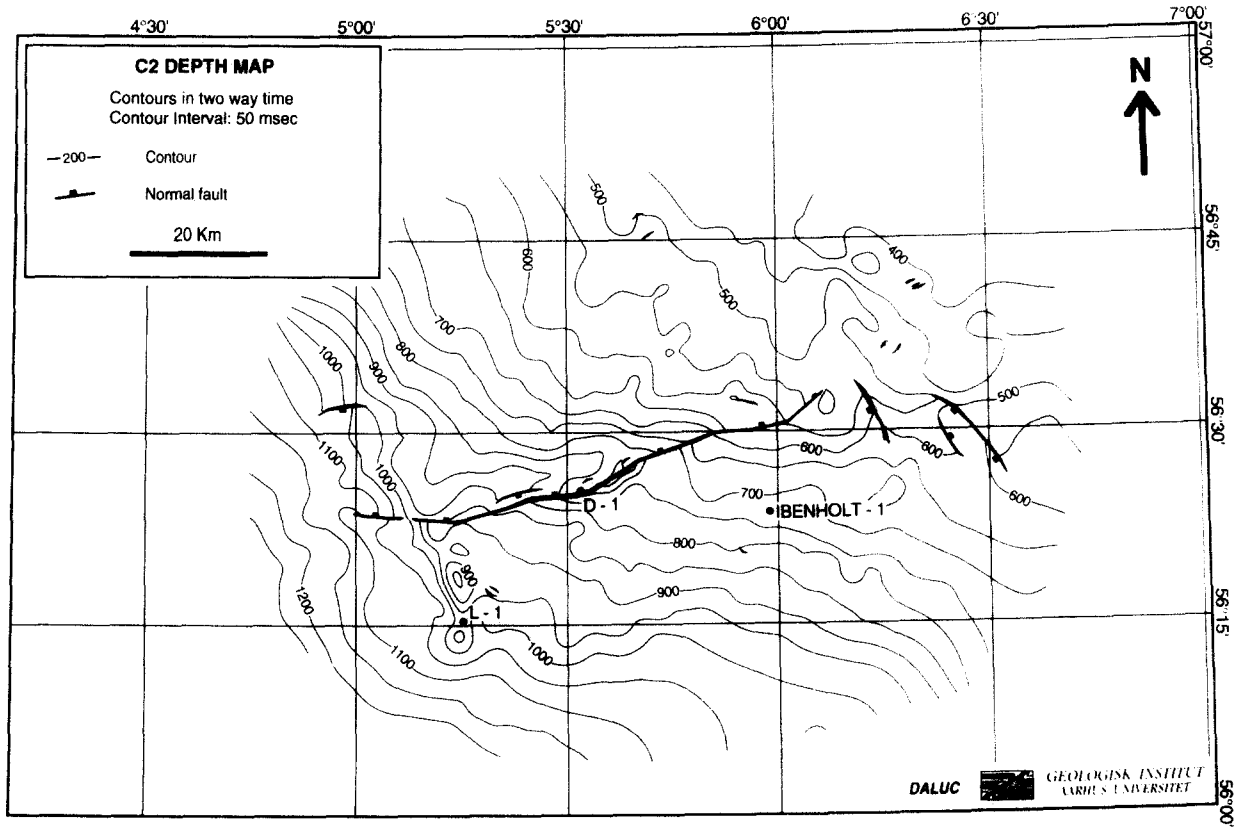

Fig. 8. Two-way time depth map to the C2 surface (Intra Early Miocene). The major fault shown is the D-1 fault.

faulting horizon; (2) the differential compaction of the beds in the hangingwall and footwall; and (3) uplift of the footwall due to shale or salt movement (footwall uplift due to elastic rebound and/or isostasy is not considered in this paper owing to the scale of the fault blocks). This method of fault displacement backstripping results in calculated displacements that are smaller than those which would be calculated by incorporating the effect of compaction. This is because the thicker sequences in the hangingwall should expand more dur-

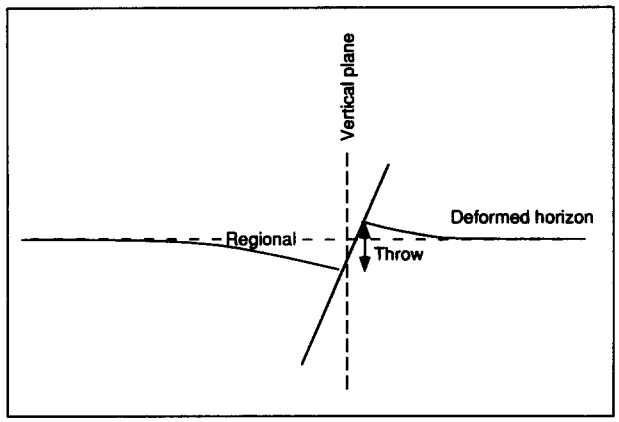

Fig. 9. Schematic diagram showing the inferred position on the projection plane of the 'regional' (see text).

ing backstripping than the corresponding and thinner sequences in the footwall. The resulting contour displacement diagram will express the minimum displacement pattern at the age considered. Thus interpretations based on these representations of the fault displacement pattern in the past might underestimate the influence of, for example, flow of salt or shale during the fault evolution.

Contour displacement diagrams for the D-1 fault have been produced for the present displacement of the Top Chalk, C1, C2 and C3 horizons as our interest is in the post-Top Chalk displacement history. The diagrams have been produced for the displacement configuration at the times of deposition of the C2 and C3 horizons (Fig. 11).

A consequence of the 'fault displacement backstripping-technique' is the progressive reduction in the number of data points which limits the level to which backstripping can be performed. Barnett *et al.* (1987) emphasized that the minimum number of measurements should be about 20 with a regular distribution of the measurements on the strike-projection. The number of regularly distributed data points in the constructed diagrams are between 42 and 70 and thus large enough to produce reliable contour displacement diagrams.

CONSTRUCTION OF VERTICAL DISPLACEMENT MAPS

The contour displacement diagrams provide information on the displacement geometry along the fault plane projection. In order to get information on the lateral variation in vertical displacement in the rock volume surrounding the growth fault, vertical displacement maps are produced. The construction of a vertical displacement map for a single horizon is based upon the present depth map and the interpreted regional; i.e. the inferred topography of the horizon if the fault was absent (Figs. 9 and 12).

The regional topography is inferred from the regional trend of depth contours outside the area affected by the fault. Figure 13 shows the Top Chalk depth map with the inferred unfaulted regional topography. Contour maps illustrating only fault displacement effects are obtained by subtracting the present surface topography of a horizon from the regional topography. This procedure effectively removes any effects of the pre-faulting horizon dip or of a later induced dip of the horizon due to regional differential subsidence, and thus emphasizes the changes in horizon geometry in the footwall and hangingwall blocks due to fault growth. Vertical displacement maps have been produced for the Top Chalk and the C2 horizons (Figs. 14 and 15).

The relationship between the location of the salt structure penetrated by the D-1 well and the area of maximum hangingwall subsidence and footwall uplift is evident by comparing the vertical displacement maps to the Top Zechstein topography (Fig. 6) which outlines the rock volume affected by near-field displacements due to fault movements.

RESULTS AND DISCUSSION

The D-1 fault may initially have developed as a blind normal fault with a 'normal' contour displacement pattern. The position of the major fault cutting the Top pre-Zechstein (Fig. 6) and the geometry of the D-1 fault (Figs. 4, 7 and 8) might suggest a physical connection between the two faults, cutting through the salt. However, the throw of the Top pre-Zechstein horizon is significantly smaller than the throw of, for example, the Top Chalk horizon, measured on depth-converted seismic sections. Furthermore, in the area surrounding the D-1 fault there is no indication of activation of basement faults in the Tertiary. Therefore, the basement fault is not likely to be directly related to the development of the D-1 fault. However, it probably triggered the formation of the salt structure in Middle Triassic times. A discussion of the formation of the salt structure is another important aspect in the understanding of the structural history of the area but is beyond the subject and scope of this study.

The initiation of the D-1 fault was probably a result of reactivation of the salt structure at the transition between Cretaceous and Tertiary time. The reactivation of salt structures in the Danish North Sea at this time is a common phenomena, probably caused by inversion tectonics and by the increased sedimentary influx in the basin following the sediment starvation in Early Cretaceous times. A continuous flow of Zechstein salt from the northwest and the southeast, accumulating beneath the footwall block, seems to have forced the fault to propagate up and down the stratigraphy changing to a more listric geometry as the fault adopted the salt surface as a detachment surface. The main fault propagation took place in post-Eocene time based on the geometry of the hangingwall and footwall sedimentary sequences.

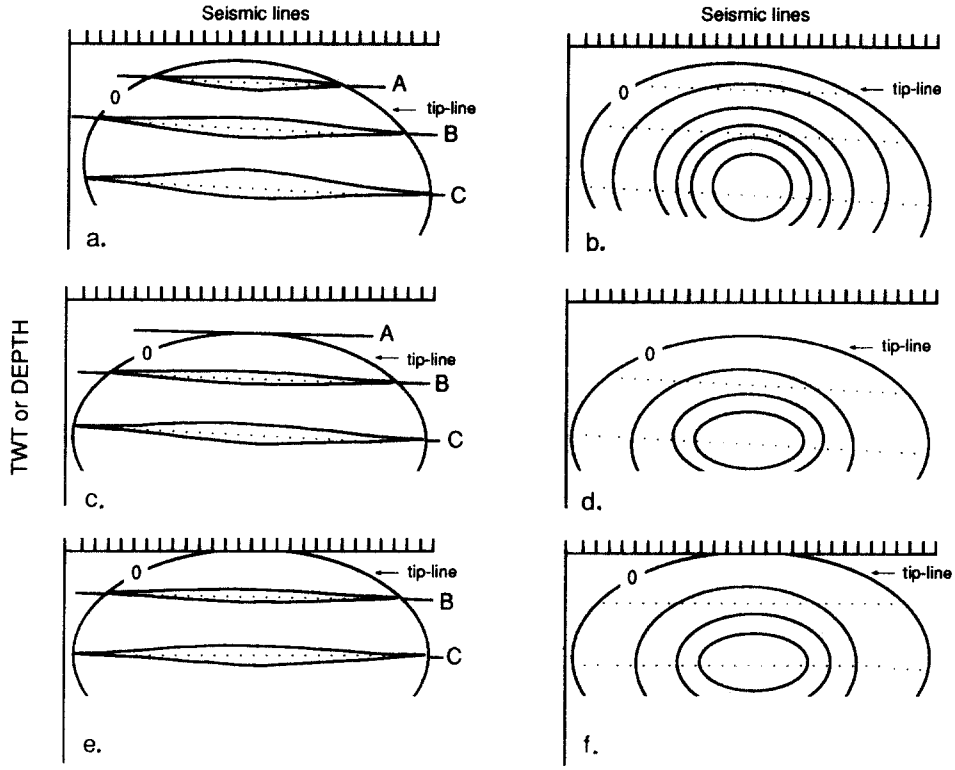

Fig. 10. Reconstruction of contour displacement diagrams (fault displacement backstripping). (a) Vertical projection along strike of fault showing the vertical displacements of three horizons cut by the same fault. The black dots indicate positions where vertical displacement have been measured. (b) The contours of vertical displacement, based on the posted displacements, show the distribution of vertical displacement on the strike projection. (c) To construct the displacement pattern at the time of deposition of horizon A the vertical displacement of horizon A is subtracted from the displacements of horizon B and C (fault displacement backstripping). (d) The resulting contour displacement diagram. (e) Finally horizons B and C are corrected for the regional subsidence since deposition of horizon A. (f) The reconstructed contour displacement diagram.

Contour displacement diagrams

Figure 11 shows contours of equal vertical displacement forming, in general, systematic and concentric semi-ellipses with a radial decrease in displacement. The smooth variation of displacement over the strike-projection makes the contour diagrams comparable to the upper half of an ideal normal blind fault (Fig. 1) and thus seems to fit the fault model of Watterson (1986), Barnett *et al.* (1987) and Walsh & Watterson (1989). It is, however, important to point out that the displacement geometries are similar but for quite different reasons. A blind fault in the sense of Barnett *et al.* (1987) is tectonic in origin whereas the formation of the D-1 fault is related to salt movement and not due to extension in the mapped area. The semi-elliptical geometry is due to the downward increase of displacement which is the expected geometrical behavior of growth faults. The maximum displacement is localized at the center of the fault and dies out towards the elliptical tip-line for all contour displacement diagrams (Fig. 11). When reconstructing the displacement pattern at various times in the past using measurements in metres the effect of compaction must be taken into account. It is beyond the scope of the present investigation to deal with this problem in detail, but it is likely that the essentials of the displacement geometry will be unchanged.

Figure 11 shows that the fault width appears to be essentially the same from C2-time until present. Removal of the displacement on the youngest horizon (horizon A in Fig. 10) will move the tip-line on the contour displacement diagram below horizon A and the minor axis will become smaller. Any reduction in the length of the long axis of the ellipse cannot be estimated by the fault displacement backstripping-technique because of absence of markers, as displacement of well-compacted rocks may be accommodated upwards by ductile deformation in unlithified sediments. The amount of displacement which should be removed because displacement in any time interval increases downwards from the fault tip is underestimated. Consequently during displacement-backstripping displacement ellipses will appear to increase their axial ratios. Watterson (1986) and Walsh & Watterson (1988) have shown that there is a systematic increase in fault dimension with increasing displacement. Although the relationship varies with rock properties and probably also with the cause of faulting it may be used to estimate the fault width at various times in the past. It is, however, also possible to estimate a more reliable location of the tip-line, graphically. The lateral displacement gradient inferred from the point of maximum displacement along the fault radius allows a construction of the approximate location of the tip-line. This causes a decrease in fault width for the displacement diagrams at progressively

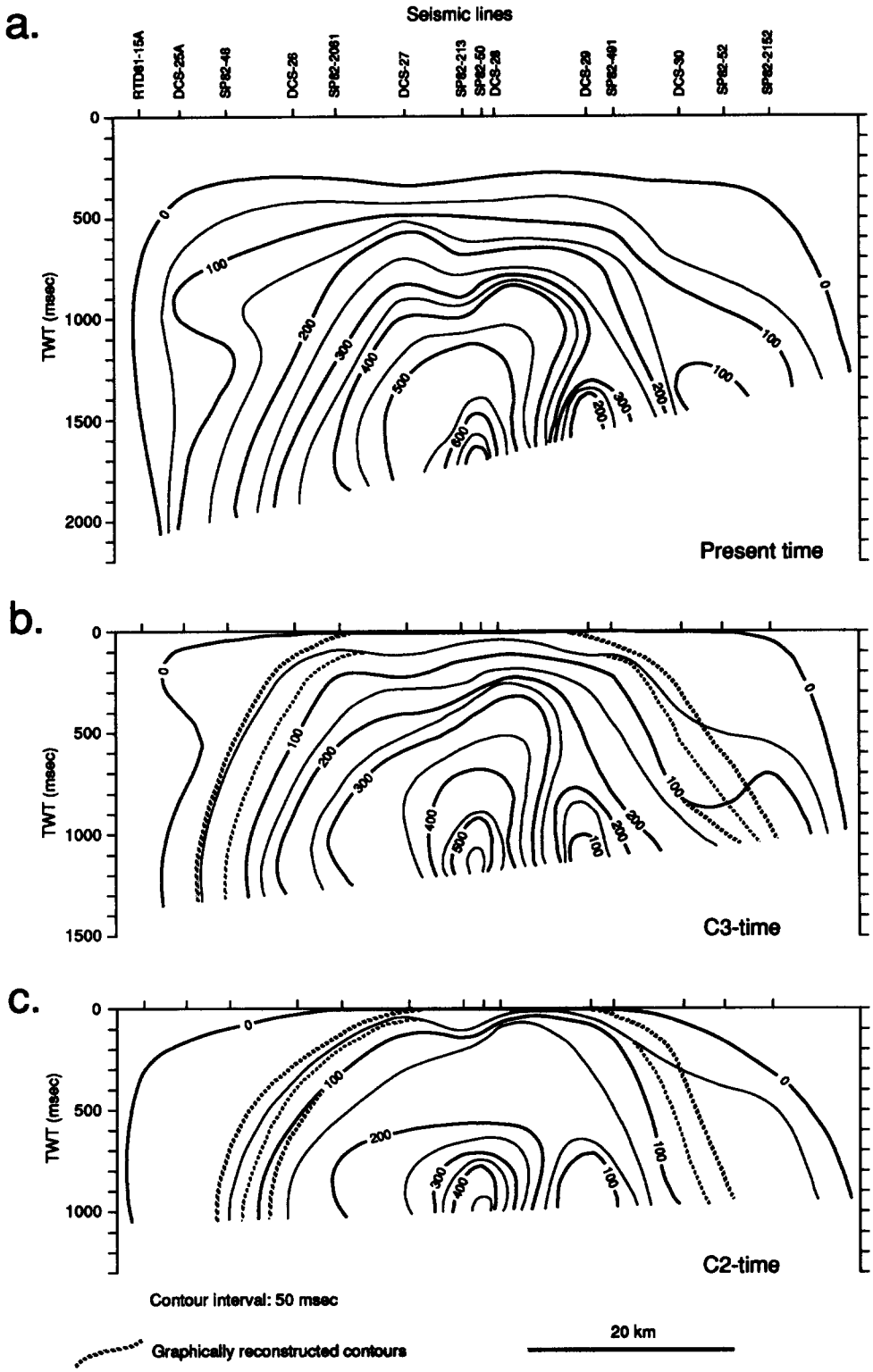

Fig. 11. Contour diagrams of equal displacement in a vertical plane parallel to the D-1 fault. Displacement values are from measurements on five mapped horizons. (a) Present displacement configuration (number of measurements $n = 70$). (b) Displacement configuration at C3-time ($n = 56$). (c) Displacement configuration at C2-time ($n = 42$). Vertical scale in two-way time. Shown in (b) and (c) are graphically estimated contours based on the displacement gradient inferred from the point of maximum displacement along the fault radius. For further discussion, see text.

earlier stages of the fault history. The position of the reconstructed tip-line at C2- and C3-time is shown in Figs. 11(b) & (c).

There is, however, a marked difference between the D-1 diagrams and the fault model of Barnett *et al.* (1987). As the D-1 fault is a growth fault it may have intersected a free surface several times during its evolution. The older the horizons, the larger is the vertical displacement since the cumulative displacement increases during the development of a growth fault. The upper half of the elliptical tip-line, i.e. the contour of zero displacement, is well defined. Due to the nature of a listric fault it is not possible to localize a near-field horizon undisturbed by the fault as the fault plane dip

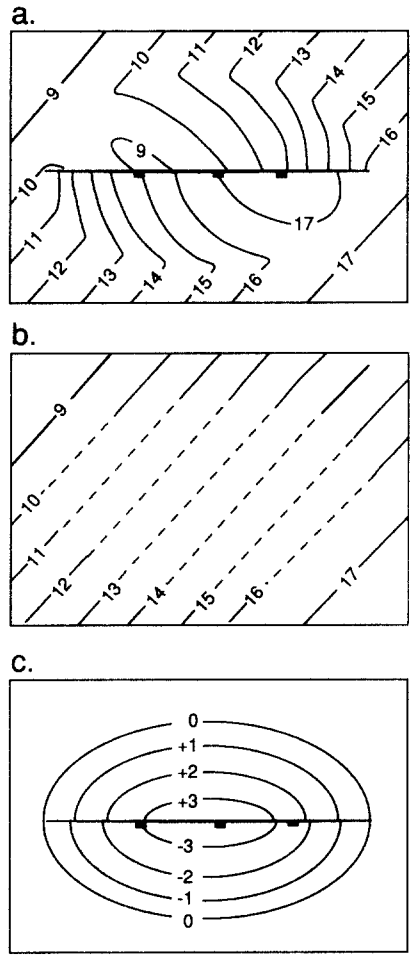

Fig. 12. Construction of a vertical displacement map for a single horizon. (a) Depth contours with arbitrary chosen contour values of a horizon cut by an ideal blind fault. (b) Reconstruction of regional topography of the horizon across the area of interest by interpolating the contours between the areas unaffected by fault-induced subsidence–uplift. (c) The vertical displacement map is obtained by subtracting map (a) from map (b). The resulting vertical displacement map shows in negative contour values the area of fault-introduced subsidence and in positive contour values in the area of fault-introduced uplift. The vertical displacement map shows the lateral variation of the vertical displacement in the rock volume surrounding the fault, unaffected by the regional subsidence introduced since the fault generation.

decreases with increasing depth approaching a flat-lying detachment surface (the Zechstein salt). Therefore, the lower half of the tip-line is undefined.

There is a marked change in the displacement geometry from C2-time until the present. The regular elliptical contour pattern (Fig. 11c) is slightly distorted between the seismic lines SP82-50 and DCS-29. The anomalously low displacement region is interpreted as an asymmetry in the fault development since C2-time. An obvious explanation is a gradual change in the flow pattern of the Zechstein salt. From Top Chalk-time until C2-time the dominant movement of salt was from below the hangingwall to below the footwall in a direction perpendicular to the fault strike. This transfer of salt from hangingwall to footwall caused a vertical movement of the salt crest below the footwall, largest at the center of the fault and gradually decreasing away from the center of the fault along the fault radius. In post C2-time movement of salt in the footwall from the east-northeast towards the center of the fault caused the distortion of the previously regular contour displacement pattern (Fig. 11).

Vertical displacement maps

The vertical displacement maps for the Top Chalk and the C2 horizons are quite similar (Figs. 14 and 15), apart from displacement values. In the hangingwall, contours of equal displacement form broad concentric semi-ellipses centered around the point of maximum displacement. In the footwall, contours are restricted to a small area at the center of the fault and form concentric semi-ellipses with major axes about one-third of the length of the hangingwall counterparts. The contours in the footwall clearly reflect the shape of the salt underlying the footwall (Fig. 6). The contour pattern approximates the synthetic contour maps for synsedimentary faults constructed by Gibson *et al.* (1989).

A marked low in the footwall contour pattern for both the Top Chalk and C2 horizons east of the center of the fault (Figs. 14 and 15), coincides with a corresponding low of the Top Zechstein surface indicating flow of salt to the southwest into the growing salt structure in post C2-time. This low in the vertical displacement maps corresponds to the low in the contour displacement diagrams as discussed above.

There is a close correspondence between the area of maximum footwall uplift and the crest of the salt structure. The reverse drag of the footwall horizons is not an elastic rebound or a product of isostatic forces but primarily an effect of salt accumulation below the footwall horizons resulting in a vertical net growth of the salt surface. The assumption that footwalls are passive (e.g. Davison 1986, White *et al.* 1986, Williams & Vann 1987, Waltham 1989) is not appropriate in the case of the salt-related D-1 fault.

CONCLUSION

The D-1 fault in the Danish North Sea has been analysed with particular attention to the nature of the displacement pattern of the listric growth fault. In particular, the interaction between the formation and development of the D-1 fault and the dynamic nature of the underlying salt structure has been investigated.

The D-1 fault initiated approximately at the transition between Cretaceous and Tertiary time, probably due to reactivation of the salt structure. The influence of the fault cutting the Top pre-Zechstein below the salt structure on the initiation of the D-1 fault is negligible.

The displacement configuration on the fault plane projection shows an overall regular fault geometry with maximum hangingwall subsidence and footwall uplift positioned at the centre of the fault and with upwards and laterally decreasing displacement. Similarly, the lateral variation of vertical displacement forms concentric semi-ellipses for the hangingwall and footwall, re-

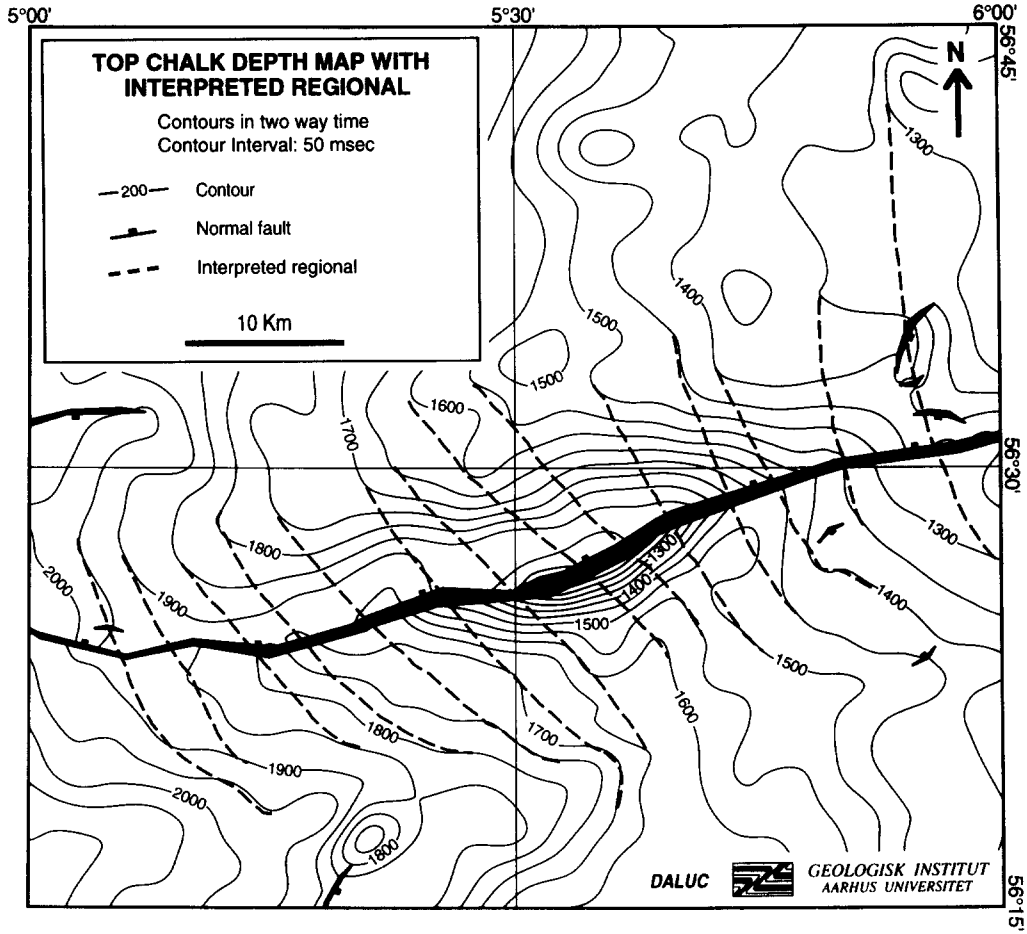

Fig. 13. Part of the Top Chalk depth map (Fig. 7) with interpreted regional topography across the D-1 fault.

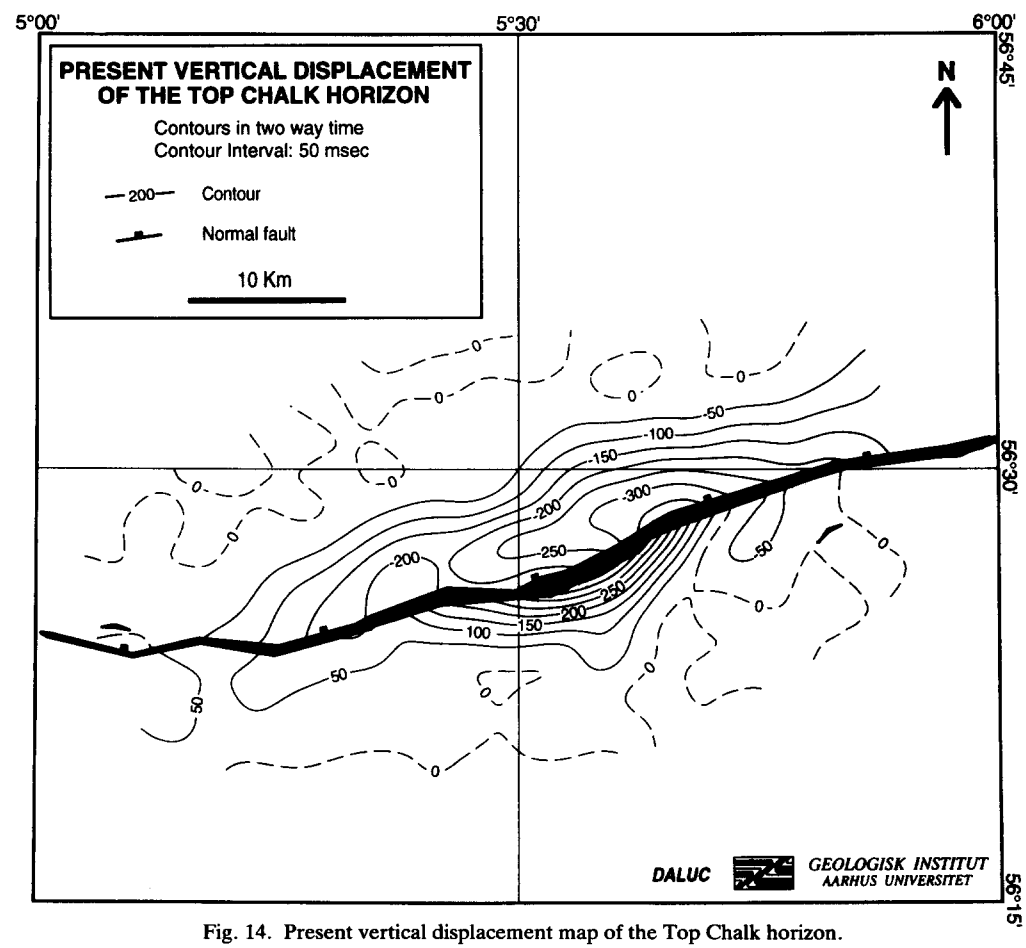

Fig. 14. Present vertical displacement map of the Top Chalk horizon.

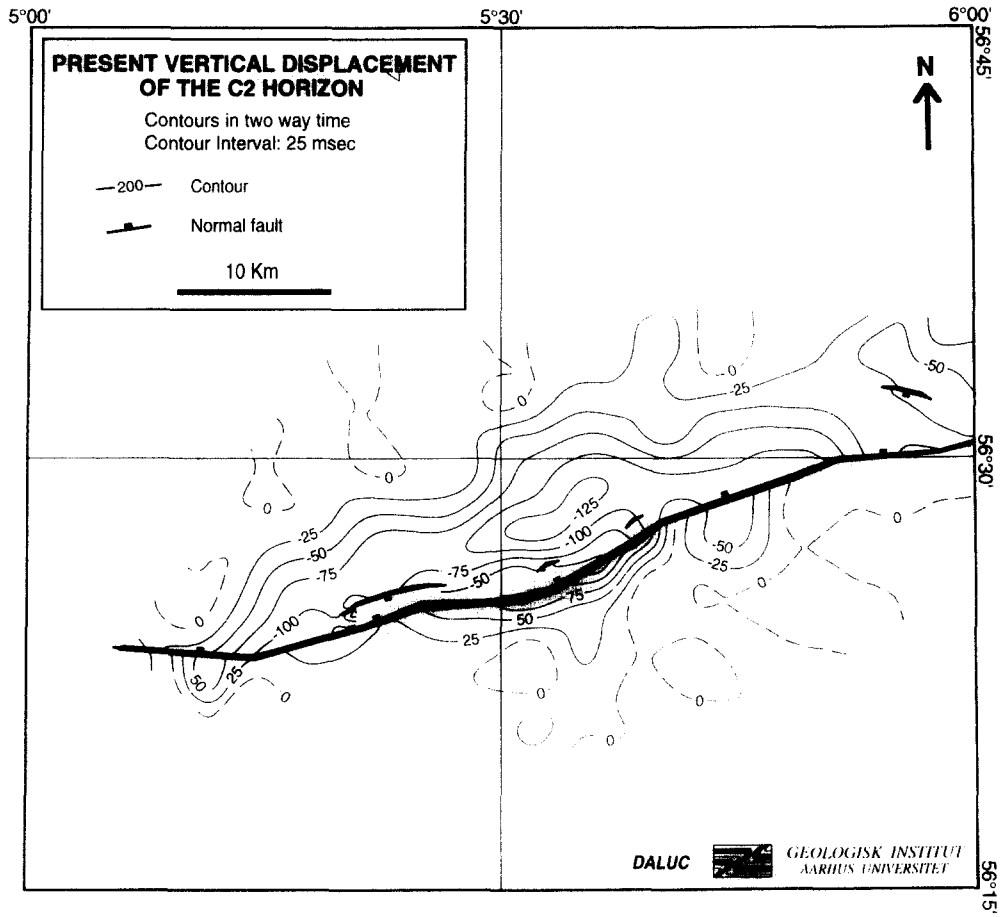

Fig. 15. Present vertical displacement map of the C2 horizon.

spectively, with the major axis of the footwall ellipse about one-third the length of the hangingwall counterpart. The location of the crest of the salt structure corresponds to the narrow central area of maximum footwall uplift.

The geometrical relationships across and around the fault, outlined by the displacement diagrams and maps, indicate that the hangingwall subsidence and footwall uplift are likely to be mainly a result of salt flow with a horizontal component towards the SW into the growing salt structure in post C2-time, superposed on the lateral salt flow perpendicular to the fault strike.

The contour diagrams of equal displacement and maps of lateral variation of the vertical displacement appear to be valuable tools in the study of the interaction between salt flow and the formation and development of the D-1 fault. Despite the complexity of salt dynamics the listric growth fault shows a regular displacement contour pattern approaching that of the upper part of an ideal simple blind fault, despite the difference in cause of fault formation. This allows additional constraints to be imposed on the interpretation of fault-related reservoir horizons across the faults located in areas influenced by salt tectonics.

Acknowledgements—This material is based upon work supported by the EC JOULE Project under contract JOUF-0036-C and by the Danish Natural Science Research Council grant No. 11-8329. We thank John J. Walsh and Juan Watterson for inspiration and constructive reviews.

REFERENCES

Barnett, J. A. M., Mortimer, J., Rippon, J. H., Walsh, J. J. & Watterson, J. 1987. Displacement geometry in the volume containing a single normal fault. *Bull. Am. Ass. Petrol. Geol.* **71**, 925–937.

Bruce, E. H. 1973. Pressured shale and related sediment deformation: mechanism for development of regional contemporaneous faults. *Bull. Am. Ass. Petrol. Geol.* **57**, 878–886.

Cater, M. C., Church, J. W., Fryer, K., Greenwood, C. W., Haskins, C. W. & Wolfenden, E. B. 1968. The micropalaeontology and stratigraphy of the Gulf Dansk Nordsø D-1 well. Robertson Research Company Limited, ARP 689-20.

Chapman, T. J. & Meneilly, A. W. 1991. The displacement patterns associated with a reverse-reactivated, normal growth fault. In: *The Geometry of Normal Faults* (edited by Roberts, A. M., Yielding, G. & Freeman, B.). *Spec. Publs geol. Soc. Lond.* **56**, 183–191.

Church, J. W., Dempsey, M., Fischer, M. J., Haskins, C. W. & Hughes, R. V. 1970. The micropalaeontology and stratigraphy of the Dansk Nordsø L-1 well. Robertson Research Company Limited, ARP 701/2652.

Crans, W., Mandl, G. & Haremboure, H. 1980. On the theory of growth faulting: a geometrical delta model based on gravity sliding. *J. Petrol. Geol.* **2**, 265–307.

Dailly, G. C. 1976. A possible mechanism relating progradation, growth faulting, clay diapirism and overthrusting in a regressive sequence of sediments. *Bull. Can. Petrol. Geol.* **24**, 92–116.

Davison, I. 1986. Listric normal fault profiles: calculation using bed-length balance and fault displacement. *J. Struct. Geol.* **8**, 209–210.

Ewing, T. E. 1983. Growth faults and salt tectonics in the Houston Diapir Province—relative timing and exploration significance. *Trans. Gulf Coast Ass. Geol. Socs* **33**, 83–90.

Frandsen, N., Vejbæk, O. V., Møller, J. J. & Michelsen, O. 1987. A geodynamic geological model of the Danish Central Trough during the Jurassic–Early Cretaceous. In: *Petroleum Geology of North West Europe*, Vol. 1 (edited by Brooks, J. & Glennie, K. W.). Graham & Trotman, London, 453–468.

Freeman, B., Yielding, G. & Badley, M. 1990. Fault correlation during seismic interpretation. *First Break* **8**, 87–95.

GECO 1989. Tectonic map of the North Sea and adjacent onshore areas. GECO Exploration Services, Surrey, U.K.

Gibson, J. R., Walsh, J. J. & Watterson, J. 1989. Modelling bed contours and cross-sections adjacent to planar normal faults. *J. Struct. Geol.* **11**, 317–328.

Gowers, M. B. & Sæbøe, A. 1985. On the structural evolution of the Central Trough in the Norwegian and Danish sectors of the North Sea. *Mar. Petrol. Geol.* **2**, 298–318.

Hamblin, W. K. 1965. Origin of "reverse drag" on the downthrown side of normal faults. *Bull. geol. Soc. Am.* **76**, 1145–1164.

Jenyon, M. K. 1986. *Salt Tectonics*. Elsevier, London.

Jenyon, M. K. 1988. Fault–salt wall relationships, southern N. Sea. *Oil and Gas J.* 5 September, 76–81.

Michelsen, O. & Andersen, C. 1981. Überblick über die regionale Geologie und Tektonik Dänemarks. *Z. angevante Geologie* **27**, 171–176.

Vejbæk, O. V. 1990. The Horn Graben, and its relationship to the Oslo Graben and the Danish Basin. In: *Rift Zones in the Continental Crust of Europe—Geophysical, Geological and Geochemical Evidence: Oslo-Horn Graben* (edited by Neumann, E.-R.). *Tectonophysics* **178**, 29–49.

Walsh, J. J. & Watterson, J. 1987. Distributions of cumulative displacement and seismic slip on a single normal fault surface. *J. Struct. Geol.* **9**, 1039–1046.

Walsh, J. J. & Watterson, J. 1988. Analysis of the relationship between displacements and dimensions of faults. *J. Struct. Geol.* **10**, 239–247.

Walsh, J. J. & Watterson, J. 1989. Displacement gradients on fault surfaces. *J. Struct. Geol.* **11**, 307–316.

Walsh, J. J. & Watterson, J. 1991. Geometric and kinematic coherence and scale effects in normal fault systems. In: *The Geometry of Normal Faults* (edited by Roberts, A. M., Yielding, G. & Freeman, B.). *Spec. Publs geol. Soc. Lond.* **56**, 193–203.

Waltham, D. 1989. Finite difference modelling of hangingwall deformation. *J. Struct. Geol.* **11**, 433–437.

Watterson, J. 1986. Fault dimensions, displacements and growth. *Pure & Appl. Geophys.* **124**, 365–373.

White, N. & Yielding, G. 1991. Calculating normal fault geometries at depth: theory and examples. In: *The Geometry of Normal Faults* (edited by Roberts, A. M., Yielding, G. & Freeman, B.). *Spec. Publs geol. Soc. Lond.* **56**, 251–260.

White, N. J., Jackson, J. A. & McKenzie, D. P. 1986. The relationship between the geometry of normal faults and that of the sedimentary layer in their hanging walls. *J. Struct. Geol.* **8**, 897–909.

Williams, G. & Vann, I. 1987. The geometry of listric normal faults and deformation in their hangingwalls. *J. Struct. Geol.* **9**, 789–795.

Ziegler, P. A. 1982. *Geological Atlas of Western and Central and Europe*. Elsevier, Amsterdam.